Case Studies in Thermal Engineering 28 (2021) 101425

Contents lists available at ScienceDirect

Case Studies in Thermal Engineering

journal homepage: www.elsevier.com/locate/csite

Optimized analysis and enhanced thermal efficiency of modified hybrid nanofluid (Al_2O_3, CuO, Cu) with nonlinear thermal radiation and shape features

A. Abbasi [a], Kamel Al-Khaled [b], M. Ijaz Khan [c,d,*], Sami Ullah Khan [e], Adel M. El-Refaey [f], Waseh Farooq [a], Mohammed Jameel [g], Sumaira Qayyum [h]

[a] Department of Mathematics, University of Azad Jammu & Kashmir, Muzaffarabad, 13100, Pakistan
[b] Department of Mathematics & Statistics, Jordan University of Science and Technology, P.O. Box 3030, Irbid, 22110, Jordan
[c] Department of Mathematics and Statistics, Riphah International University, I-14, Islamabad, 44000, Pakistan
[d] Nonlinear Analysis and Applied Mathematics (NAAM) Research Group, Department of Mathematics, Faculty of Science, King Abdulaziz University, P.O. Box 80257, Jeddah, 21589, Saudi Arabia
[e] Department of Mathematics, COMSATS University Islamabad, Sahiwal, 57000, Pakistan
[f] Department of Basic and Applied Science, College of Engineering and Technology, Arab Academy for Science, Technology & Maritime Transport, Smart Village Campus, Cairo, Egypt
[g] Department of Civil Engineering, College of Engineering, King Khalid University, Abha, Saudi Arabia
[h] Department of Mathematics, Quaid-I-Azam University 45320, Islamabad, 44000, Pakistan

ARTICLE INFO

Keywords:
Modified hybrid nanofluid
Entropy generation
Shape effects
Viscous dissipation
Thermal radiation

ABSTRACT

The thermal characteristics of modified hybrid nanoparticles have been studied between two parallel walls with applications of entropy generation and nonlinear thermal radiation. Three types of nanoparticles namely copper oxide (CuO), copper nanoparticles (Cu) and aluminum oxide (Al_2O_3) are utilized to thermal determination of heat transfer. The contribution of viscous dissipation and Joule heating is also inspected. Moreover, the shape effects for the three types of nanoparticles are addressed as a novelty. The mathematical model is developed in view of associated laws and thermal properties of modified hybrid nanofluid. The problem is first modeled in terms of partial differential equations for which the similarity variables are followed to convert the system into dimensionless form. The Keller box numerical scheme is used to obtain the solution. The thermo-physical properties of nanoparticles and fluctuation in the heat transfer rate are reported for the flow parameters. The results claimed that the temperature profile enhanced solid volume faction of copper oxide nanoparticles. A lower change in the entropy generation is observed for the solid volume fraction of aluminum oxide and copper nanoparticles.

1. Introduction

The heat transfer is one of the primary and most important phenomenon in various engineering and industrial sectors. Many engineering and industrial processes like extrusion processes, electronic cooling, refining industry, micro heat pipes, premium thermal

* Corresponding author. Nonlinear Analysis and Applied Mathematics (NAAM) Research Group, Department of Mathematics, Faculty of Science, King Abdulaziz University, P.O. Box 80257, Jeddah, 21589, Saudi Arabia.
E-mail address: ijazfmg_khan@yahoo.com (M.I. Khan).

https://doi.org/10.1016/j.csite.2021.101425
Received 10 July 2021; Received in revised form 30 August 2021; Accepted 4 September 2021
Available online 16 September 2021
2214-157X/© 2021 Published by Elsevier Ltd. This is an open access article under the CC BY-NC-ND license (http://creativecommons.org/licenses/by-nc-nd/4.0/).

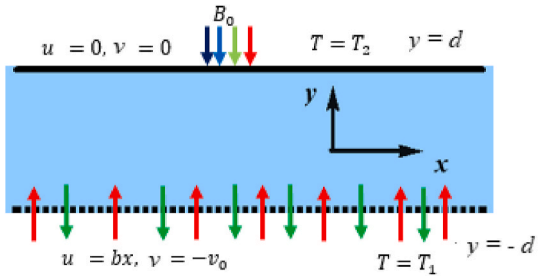

Fig. 1. Flow sketch.

oil, micro-heat pipe arrays conveys the role of heat of transfer [1–3]. In most of heavy industries, the base fluids are used as a source of energy. However, the thermal capability of many bas liquids is quite limited and fails to fulfill the industrial requirements. The interaction of nanofluids is considered as an alternative source of energy and attained the researcher focus in very short time. The thermal dynamic of nanoparticles is extremely interesting and novel from the applications point of view. Following to the multidisciplinary nature and ultra peak thermal characteristics, the nanoparticles are recently used in distinct industrial and engineering sectors like heating processes, sustainable manufacturing, automotive, extrusion mechanism, thin-film, solar systems, petroleum refining, automotive catalytic converters, air purifiers, chemical processes, antibacterial cleansers etc. The nanoparticles more superior as compared to the base materials due to dominant thermal properties. Choi [4] initiated the basic work on the nanoparticles with experimental justifications. Ramesh et al. [5] focused on the thermal utilization of copper and aluminum nanoparticles with water base fluid due to convectively moving surface. Ahmad and Nadeem [6] considered the thermal inspection of nanoparticles subject to the Hall features and ion current. Raza et al. [7] focused on the optimized analysis of copper nanoparticles channel with porous walls. Gangadhar et al. [8] discussed the importance of Newtonian heating on the micropolar nanofluid flow under the implementation of magnetic force. Gangadhar et al. [9] investigated the engine oil thermal inspection for the wedge surface flow numerically via Keller box scheme. Ali et al. [10] explored the activation energy and buoyancy forces impact for the Maxwell nanofluid due to moving wedge. Hosseinzadeh et al. [11] determined the bioconvection thermal mechanism for cross nanofluid flow in three-dimensional moving cylinder. Song et al. [12] identified the micropolar nanoparticles thermal significances for the off centered flow of disk with modified Darcy porous relations. Gangadhar et al. [13] focused on the internal heat generation of nanofluid with microorganisms. Dasaradha et al. [14] addressed the heat transfer involvement for the rotating flow of Maxwell nanofluid via non-Fourier heat flux model. The spectral relaxation numerical computations for the nanofluid problem were intended by Gangadhar et al. [15]. Turkyilmazoglu [16] visualized the heat transfer determination for the nanofluid flow accounted by a moving substrate.

The thermal optimization of different extrusion and engineering processes is quite necessary for the enhancement of energy production. Different thermodynamics laws are followed for the explaining the heat determination and extrusion processes. Based on the statement of first thermodynamics theory, the transmission of energy within medium is changed and transformed to different systems without any energy loss. This law helps the scientists to develop various thermal models. However, the major drawback of first thermodynamics theory is that its fails to justify the irreversibilities (entropy generation). On this end, second law of thermodynamics justified the availability and collection of energy consumptions and subsequently reduces the loss in the energy. Bejan [17] presented the basic investigation for the entropy generation analysis regarding the heat transfer. Ijaz et al. [18] presented the physical aspects of radiated Sisko nanoparticles along with bioconvection and entropy generation. Hosseinzadeha et al. [19] reported the optimized significances for carbon nanotubes with the essential role of thermal radiation. Nayak et al. [20] observed the entropy generation features while determining the thermal onset of Hamilton's Crosser nanofluid model. This research also directs the shape factor effects of nanoparticles and interfacial layer concept. The involvement of entropy generation for the chemical reactive nanoparticles flow has been theoretically evaluated by Khan et al. [21]. Qureshi et al. [22] observed the entropy generation phenomenon for the hybridized nanofluid for the orthogonal coaxial disks. Li et al. [23] estimated the framework of entropy generation for the viscous nanoparticles flow induced via rotating cone. Mondal and Mahapatra [24] investigated the entropy generation transportation in trapezoidal cavity compiling with nanoparticles. Usman et al. [25] investigated the power law nanofluid thermal achievement for the rotator disk along with the porous space. Batool et al. [26] conducted the research on the entropy generation phenomenon of nanofluids with the double diffusion aspects. Sattar et al. [27] worked out the entropy generation flow in the wavy cavity for the nanoparticles along with novel thermophysical prospective. Le et al. [28] discussed the entropy generation involvement and applications for the Jeffrey nanofluid flow in presence of slip effects. Refs. [29–33] signifies some new developments in fluid flow subject to different shape geometries.

Table 1
Thermal properties of modified hybrid nanofluid.

Properties	Hybrid nanofluid
Density	$\rho_{mnf} = (1-\varphi_3)\{(1-\varphi_2)[(1-\varphi_1)\rho_f + \varphi_1\rho_{s_1}] + \varphi_2\rho_{s_2}\} + \varphi_3\rho_{s_3}$
Dynamic viscosity	$\mu_{mnf} = \frac{\mu_f}{(1-\varphi_1)^{2.5}(1-\varphi_2)^{2.5}(1-\varphi_3)^{2.5}}$
Heat capacity	$(\rho C_p)_{mnf} = (1-\varphi_3)\left\{(1-\varphi_2)\left[\begin{matrix}(1-\varphi_1)(\rho C_p)_f \\ +\varphi_1(\rho C_p)_{s_1}\end{matrix}\right] + \varphi_2(\rho C_p)_{s_2}\right\} + \varphi_3(\rho C_p)_{s_3}$
Thermal conductivity	$\frac{k_{mnf}}{k_{hnf}} = \frac{k_{s_3} + (m-1)k_{hnf} - (m-1)\varphi_3(k_{hnf} - k_{s_3})}{k_{s_3} + (m-1)k_{hnf} + \varphi_3(k_{hnf} - k_{s_3})}$, Where $\frac{k_{hnf}}{k_{nf}} = \frac{k_{s_2} + (m-1)k_{nf} - (m-1)\varphi_2(k_{nf} - k_{s_3})}{k_{s_2} + (m-1)k_{nf} + \varphi_2(k_{nf} - k_{s_3})}$, and also $\frac{k_{nf}}{k_f} = \frac{k_{s_1} + (m-1)k_f - (m-1)\varphi_1(k_f - k_{s_1})}{k_{s_3} + (m-1)k_f + \varphi_1(k_f - k_{s_1})}$.
Electric conductivity	$\frac{\sigma_{mnf}}{\sigma_{hnf}} = \frac{\sigma_{s_3} + 2\sigma_{hnf} - 2\varphi_3(\sigma_{hnf} - \sigma_{s_3})}{\sigma_{s_3} + 2\sigma_{hnf} + \varphi_3(\sigma_{hnf} - \sigma_{s_3})}$ where $\frac{\sigma_{mnf}}{\sigma_{hnf}} = \frac{\sigma_{s_2} + 2\sigma_{nf} - 2\varphi_2(\sigma_{nf} - \sigma_{s_2})}{\sigma_{s_2} + 2\sigma_{nf} + \varphi_2(\sigma_{nf} - \sigma_{s_2})}$ and also $\frac{\sigma_{nf}}{\sigma_f} = \frac{\sigma_{s_1} + 2\sigma_f - 2\varphi_1(\sigma_f - \sigma_{s_1})}{\sigma_{s_1} + 2\sigma_f + \varphi_1(\sigma_f - \sigma_{s_1})}$.

Table 2
The shape factor for different nanoparticles.

Different shapes of nanoparticles	Numerical values
Blades	8.6
Platelets	5.7
Cylinders	4.9
Bricks	3.7

Following to the interesting thermal physical properties of nanoparticles in presence of entropy generation phenomenon, this research communicates the optimized flow of modified hybrid nanoparticles in presence of Joule heating and viscous dissipation. The modified nanoparticles consists of three types of nanoparticles namely copper oxide (CuO), copper nanoparticles (Cu) and aluminum oxide (Al_2O_3) nanoparticles are utilized to inspect the thermal performances. The modeling and applications of entropy generation for these nanoparticles are inspected. The interesting features of Joule heating, viscous dissipation and nonlinear thermal radiation are also observed to make the model more novel and versatile. Moreover, the shape features are studied for utilized nanoparticles. After the modeling and simulations, the shooting technique is employed for the numerical calculations. A detailed analysis regarding the properties, shape features and thermal aspects of nanoparticles is graphically studied.

2. Formulation of the problem

In present computational model, we use steady, incompressible and two dimensional flow of modified nanofluid between two parallel walls. The flow is considered along $x-axis$ while $y-axis$ is orthogonal to flow. The lower plate is at $y=-d$ is stretched with linear velocity ax and is porous while upper plate at $y=d$ is at rest and non-spongy. The flow of modified nanofluid is also considered under the subject of strong magnetic field having strengthB_0. Furthermore, the effects of non-linear thermal radiation and Ohmic heating are also taken into account. The systematic flow sketch is presented in Fig. 1. Under the above assumptions the governing equations of motion following are [7]:

$$\frac{\partial u}{\partial x}+\frac{\partial v}{\partial y}=0, \tag{1}$$

$$\rho_{mnf}\left(u\frac{\partial u}{\partial x}+v\frac{\partial u}{\partial y}\right)=-\frac{\partial p}{\partial x}+\mu_{mnf}\left(\frac{\partial^2 u}{\partial x^2}+\frac{\partial^2 u}{\partial y^2}\right)-\sigma_{mnf}B_0^2u, \tag{2}$$

Table 3
Numerical values of physical properties of base fluid and nanoparticles.

Base fluid/Solid particles	$\rho(Kgm^3)$	$C_p(JKg^{-1}K^{-1})$	$k(Wm^{-1}K^{-1})$	$\sigma(\Omega m)^{-1}$
H_2O	997.1	4180	0.6071	5.5×10^{-6}
$Al_2O_3(\varphi_3)$	3970	765	40	35×10^{6}
$Cu(\varphi_2)$	8933	385	400	59.6×10^{6}
$CuO(\varphi_1)$	6500	540	18	6.9×10^{-2}

$$\rho_{mnf}\left(u\frac{\partial v}{\partial x}+v\frac{\partial v}{\partial y}\right)=-\frac{\partial p}{\partial y}+\mu_{mnf}\left(\frac{\partial^2 v}{\partial x^2}+\frac{\partial^2 v}{\partial y^2}\right), \tag{3}$$

The energy equation with the effects of Ohmic heating, viscous dissipation and non-linear thermal radiation is:

$$\left(\rho C_p\right)_{mnf}\left(u\frac{\partial T}{\partial x}+v\frac{\partial T}{\partial y}\right)=k_{hnf}\left(\frac{\partial^2 T}{\partial x^2}+\frac{\partial^2 T}{\partial y^2}\right)+\Phi+\sigma_{mnf}B_0^2u^2-\frac{\partial q_r}{\partial y}. \tag{4}$$

In the above equations u is velocity component along $x-axes$ and$v$ is velocity component along $y-axes$. The term Φ arises in equation (4) due to viscous dissipation and for Newtonian fluid can be expressed as:

$$\Phi=\mu_{mnf}\left[2\left(\left(\frac{\partial u}{\partial x}\right)^2+\left(\frac{\partial v}{\partial y}\right)^2\right)+\left(\frac{\partial u}{\partial y}+\frac{\partial v}{\partial x}\right)^2\right]. \tag{5}$$

where q_r is Radiative heat flux and is defined as Abbasi et al. [25].

$$q_r=-\frac{4}{3}\frac{\sigma_1}{(\sigma_r-\sigma_s)}\frac{\partial T^4}{\partial y}. \tag{6}$$

where $\sigma_1$is Stefan-Boltzmann constant and σ_r are mean absorption coefficient and σ_s is scattering coefficient, respectively. ρ_{mnf} is effective density, μ_{mnf} is effective viscosity, $(\rho C_p)_{mnf}$ is heat capacity and k_{mnf} is thermal conductivity of modified nanofluid.

The thermal properties in terms of mathematical relations are presented in Table 1.

In Table 1, φ_1 is volume fraction of CuO, φ_2 is volume fraction of Cu and φ_3 is volume fraction of Al_2O_3 nanoparticles. Subscripts s_1, s_2 and s_3 stands for denoting the properties of CuO, Cu and Al_2O_3 nanoparticles. Furthermore, m is the shape factor for which the numerical values are presented for various shape factors in Table 2.

Subject to the appropriate boundary conditions

$$\left.\begin{array}{l} u=ax, v=v_0, T=T_1 aty=-d \\ u=0, v=0, T=T_2 aty=d \end{array}\right\}. \tag{7}$$

In which $a<0$ represents shrinking wall of the channel while $a>0$ represents for stretching wall case. Now in order to facilitate the solution we use the similarity transformations [24] as used:

$$\eta=\frac{y}{d},\ u=axf'(\eta), v=-adf(\eta),\ \theta(\eta)=\frac{T-T_2}{T_1-T_2}. \tag{8}$$

After using the similarity transformations as defined above, equations (1)–(4) in dimensionless form takes the form

$$f^{iv}-B_1BRe(f'f''-ff''')-M^2BB_2f''=0, \tag{9}$$

$$\frac{1}{PrRe}\left(\left(1+\frac{4}{3}\frac{Rn}{B_4}(1+(\omega-1)\theta(\eta))^3\right)\theta'\right)'+\frac{B_3}{B_4}f\theta'+\frac{Ec}{Re}\left(\begin{array}{l}\frac{1}{B_4B}\left(4f'^2+\delta_1 f''^2\right)\\ +\frac{B_2}{B_4}M^2f'^2\end{array}\right)=0. \tag{10}$$

The boundary conditions in dimensionless form are

$$\left.\begin{array}{l} f^{'}(-1)=1, f(-1)=\beta, \theta(-1)=1 \\ f^{'}(1)=0, f(1)=0, \theta(1)=0 \end{array}\right\}. \tag{11}$$

In which $M^2=\sigma_f B_0^2 d^2/\mu_f$ is magnetic parameter, $Re=d^2a/\nu_f$ is Reynolds number, $Pr=d^2a(\rho C_p)_f/k_f$ is Prandtl number, $Rn=4\sigma_1 T_2^3/(3k_f)(\sigma_r+\sigma_s)$ is radiation parameter, δ_1 is dimensionless constant and $\beta=v_0/da$is suction parameter. Also, B, B_1, B_2, B_3 and $B_4$are constants and defined as

$$B=(1-\varphi_1)^{2.5}(1-\varphi_1)^{2.5}(1-\varphi_1)^{2.5}, \tag{12}$$

$$B_1=\frac{\rho_{mnf}}{\rho_f}=(1-\varphi_3)\left\{(1-\varphi_2)\left[(1-\varphi_1)+\varphi_1\frac{\rho_{s_1}}{\rho_f}\right]+\varphi_2\frac{\rho_{s_2}}{\rho_f}\right\}+\varphi_3\frac{\rho_{s_3}}{\rho_f}, \tag{13}$$

$$B_2=\frac{\sigma_{mnf}}{\sigma_f}=\frac{\sigma_{s_3}+2\sigma_{hnf}-2\varphi_3(\sigma_{hnf}-\sigma_{s_3})}{\sigma_{s_3}+2\sigma_{hnf}+\varphi_3(\sigma_{hnf}-\sigma_{s_3})}*\frac{\sigma_{s_2}+2\sigma_{nf}-2\varphi_2(\sigma_{nf}-\sigma_{s_2})}{\sigma_{s_2}+2\sigma_{nf}+\varphi_2(\sigma_{nf}-\sigma_{s_2})}*\frac{\sigma_{s_1}+2\sigma_f-2\varphi_1(\sigma_f-\sigma_{s_1})}{\sigma_{s_1}+2\sigma_f+\varphi_1(\sigma_f-\sigma_{s_1})}, \tag{14}$$

$$B_3=\frac{(\rho C_p)_{mnf}}{(\rho C_p)_f}=(1-\varphi_3)\left\{(1-\varphi_2)\left[(1-\varphi_1)+\varphi_1\frac{(\rho C_p)_{s_1}}{(\rho C_p)_f}\right]+\varphi_2\frac{(\rho C_p)_{s_2}}{(\rho C_p)_f}\right\}+\varphi_3\frac{(\rho C_p)_{s_3}}{(\rho C_p)_f}, \tag{15}$$

$$B_4=\frac{k_{mnf}}{k_f}=\frac{k_{s_3}+(m-1)k_{hnf}-(m-1)\varphi_3(k_{hnf}-k_{s_3})}{k_{s_3}+(m-1)k_{hnf}+\varphi_3(k_{hnf}-k_{s_3})}*\frac{k_{s_2}+(m-1)k_{nf}-(m-1)\varphi_2(k_{nf}-k_{s_3})}{k_{s_2}+(m-1)k_{nf}+\varphi_2(k_{nf}-k_{s_3})}*\frac{k_{s_2}+(m-1)k_{nf}-(m-1)\varphi_2(k_{nf}-k_{s_3})}{k_{s_2}+(m-1)k_{nf}+\varphi_2(k_{nf}-k_{s_3})}. \tag{16}$$

The numerical illustration of base fluid and nanoparticles is presented in Table 3.

2.1. Engineering interest quantities

The skin fraction coefficient $C_f$and Nusselt number Nu at $y=-d$can be defined as

$$C_f=\frac{\mu_{mnf}}{\rho_f(bx)^2}\left(\frac{\partial u}{\partial y}\right)_{y=-h} \text{ and } Nu=-\frac{1}{k_f(T_1-T_2)}\left(k_{mnf}\frac{\partial T}{\partial y}+\frac{4}{3}\frac{\sigma_1}{(\sigma_r-\sigma_s)}\frac{\partial T^4}{\partial y}\right)_{y=-h}. \tag{17}$$

In dimensionless form, above expressions takes the form

$$Re_x^{1/2}C_f=\frac{1}{A}f''\left(-1\right) \text{and } Re_x^{1/2}Nu=-\left(A_4+Rn(1+(\omega-1)\theta(-1))^3\right)\theta^{'}(-1) \tag{18}$$

2.2. Entropy generation

Entropy generation abrogates the available energy in the framework of few industrial and engineering processes. It is, therefore, worthwhile to discover in a framework the rate of entropy production. The volumetric rate of local entropy generation of viscous fluid is defined as [22]:

$$S_G=\frac{k_{mnf}}{T_1^2}\left(\left(\frac{\partial T}{\partial x}\right)^2+\left(\frac{\partial T}{\partial y}\right)^2\right)+\frac{\Phi}{T_1}+\frac{\sigma_{mnf}B_0^2}{T_1}u^2+\frac{1}{T_1^2}\frac{4}{3}\frac{\sigma_1}{(\sigma_r-\sigma_s)}T^3\left(\frac{\partial T}{\partial y}\right)^2, \tag{19}$$

In the above Eq. (18), the first term characterizes the irreversibility due to heat transfer, second term epitomize the irreversibility due to fluid friction, third term due to joule heating and last term corresponds to thermal radiation. N_sPortrays the dimensionless entropy production and is identified as

$$N_s=\frac{d^2T_1^2}{k_f(T_1-T_2)^2}S_G, \tag{20}$$

The dimensionless entropy generation arises after using the transformations in (7), we have

$$N_s = \frac{1}{\Omega}\left(\begin{array}{l} A_2 M^2 PrEc(f'(\eta))^2 \\ +\frac{PrEc}{A}\left(4(f'(\eta))^2 + \delta_1 (f''(\eta))^2\right) \end{array}\right) + \begin{array}{l} A_4(\theta'(\eta))^2 + \\ Rn(1+(\omega-1)\theta(\eta))^3(\theta'(\eta))^2 \end{array} \tag{21}$$

Bejan number is described as the proportional of the entropy minimization due to thermal irreversibility to the total entropy optimization, and in present study the Bejan number (Be) can be defined as

$$Be = \frac{(A_4)(\theta'(\eta))^2 + Rn(1+(\omega-1)\theta(\eta))(\theta'(\eta))^2}{\frac{1}{\Omega}\left(\begin{array}{l} A_2 M^2 PrEc(f'(\eta))^2 \\ +\frac{PrEc}{A}\left(4(f'(\eta))^2 + \delta_1 (f''(\eta))^2\right) \end{array}\right) + \begin{array}{l} A_4(\theta'(\eta))^2 + \\ Rn(1+(\omega-1)\theta(\eta))^3(\theta'(\eta))^2 \end{array}}, \tag{22}$$

where $\Omega = \frac{T_1 - T_2}{T_1}$.

3. Solution methodology

Due to the non-linearity of the system of equations 9 and 10 subject to the boundary conditions, it is difficult to report analytical solution. Many numerical techniques are reported by researchers to compute such type of equations describing the flow phenomena under different assumptions. A two point implicit finite difference scheme with second order accuracy which is unusually known as Keller box method. This is due to the fact that the finite difference equations incorporate both specified initial and terminal conditions in the final set of equations, and thus the resulting solutions of these equations are constrained to satisfy these boundary conditions. This differs from a shooting method, where the terminal boundary condition never enters into the solution during the forward integration process. Another difference is that the solution is produced simultaneously at all points, whereas in a shooting method the solutions at different points are generated in sequence. We may therefore expect the solutions near the terminal point to be less accurate than those obtained near the initial point because of the propagation of round-off errors. In first step of this method we resolve the equations in (9-10) into corresponding first order equations. For this let

$$f' = U, U' = V, V' = W, \theta' = Y, \tag{23}$$

We can write (9-10) as

$$W' - B_1 BRe(UV - fW) - M^2 BB_2 V = 0, \tag{24}$$

$$\frac{1}{PrRe}\left(\left(1 + \frac{4}{3}\frac{Rn}{B_4}(1+(\omega-1)\theta(\eta))^3\right)Y\right)' + \frac{B_3}{B_4} fY + \frac{Ec}{Re}\left(\begin{array}{l} \frac{1}{B_4 B}\left(4U^2 + \delta V^2\right) \\ +\frac{B_2}{B_4} M^2 U^2 \end{array}\right) = 0. \tag{25}$$

The main advantage of this finite difference method is to compute no-longer unwanted values of f_j and θ_j i.e. $f_{-1}, U_{-1}, V_{-1}, f_{j+1}, Y_{-1}$ etc.

In second step, the derivative of all dependent variables by central difference and rest of quantities by taking averaging. equations 23–25 takes the form

$$\left.\begin{array}{l} \frac{f_j - f_{j-1}}{h_j} = U_{j-\frac{1}{2}} \\ \frac{U_j - U_{j-1}}{h_j} = V_{j-\frac{1}{2}} \\ \frac{V_j - V_{j-1}}{h_j} = W_{j-\frac{1}{2}} \\ \frac{\theta_j - \theta_{j-1}}{h_j} = Y_{j-\frac{1}{2}} \end{array}\right\}, \tag{26}$$

$$\frac{W_j - W_{j-1}}{h_j} - B_1 BRe\left(U_{j-\frac{1}{2}} V_{j-\frac{1}{2}} - f_{j-\frac{1}{2}} W_{j-\frac{1}{2}}\right) - M^2 BB_2 V_{j-\frac{1}{2}} = 0, \tag{27}$$

Table 4
Comparative analysis of obtained results with Raza et al. [7].

Parameters					$f''(-1)$ when $(\varphi_1 = \varphi_3 = 0.0)$	
Re	*M*	*Pr*	β	φ_2	Present	Raza et al. [7]
		1.0	0.5	0.0	− 9.384763	− 9.384752739
				0.01	− 9.846195	− 9.846596801
				0.03	− 10.720627	− 10.71745956
	0.0				− 10.75679516	− 10.75677730

Table 5
Variation of Skin fraction $Re_x^{1/2}\, C_f$ and Nusselt number $Re_x^{1/2}\, Nu$when$Rn = 1, 0., Ec = 0.5, m = 8.6, \delta_1 = 0.5, \omega = 1.5$ and.$Pr = 6.2$.

Parameters			$(Cu+Al_2O_3)$ Hybrid nanofluid $(\varphi_1 = 0, \varphi_2 = \varphi_2 = 0.04)$		$(CuO+Cu+Al_2O_3)$ modified nanofluid $(\varphi_1 = \varphi_2 = \varphi_2 = 0.04)$	
M	β	*Re*	$Re_x^{1/2} C_f$	$Re_x^{1/2} Nu$	$Re_x^{1/2} C_f$	$Re_x^{1/2} Nu$
0.1	0.5	10	− 13.355450	19.471419	− 15.394072	17.102310
0.5			− 13.293855	19.973557	− 15.314709	17.751980
1.0			− 13.150696	21.075536	− 15.126019	19.154620
	0.1		− 5.729520	9.812102	− 6.441298	9.423768
	0.2		− 6.988689	13.422713	− 7.894949	12.887788
	0.4		− 10.595658	19.429602	− 12.102862	18.256182
		1.0	− 4.010664	− 1.158827	− 4.434659	− 1.645399
		3.0	− 5.231213	1.785631	− 5.850892	1.080936
		5.0	− 6.617058	6.486399	− 7.462549	5.560531

Table 6
Variation of Nusselt number $Re_x^{1/2}\, Nu$ when $Pr = 6.2, m = 8.6$ and.$\delta_1 = 0.5$.

Parameters					$Re_x^{1/2} Nu$	
M	β	*Re*	*Rn*	*Ec*	$\omega = 1.0$	$\omega = 1.5$
0.1	0.5	10	1.0	0.5	17.789337	17.102310
0.5					18.322908	17.751980
1.0					19.480259	19.154620
	0.1				8.502479	9.423769
	0.2				12.145977	12.887788
	0.4				18.078251	18.256183
		1.0			− 2.599965	− 1.645399
		3.0			0.667606	1.080936
		5.0			5.542184	5.560532
			0.1		7.246929	12.654992
			0.4		6.532423	7.884829
			0.8		5.829779	6.296412
				0.1	13.586704	14.873717
				0.2	11.646158	12.710056
				0.3	9.706488	10.553414

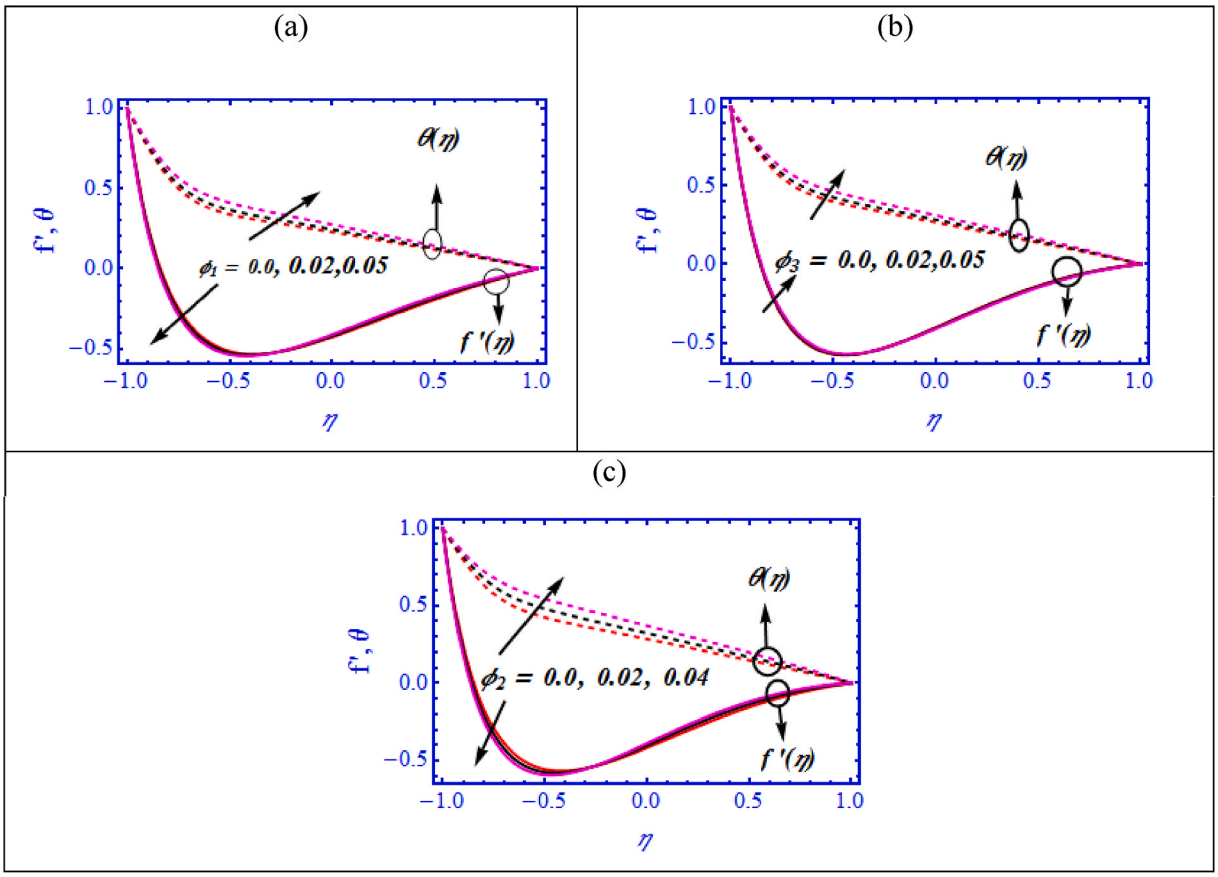

Fig. 2. (a) Change in $f^{'}$ and θ for solid volume fraction of *CuO*, (b)Change in $f^{'}$ and θ for solid volume fraction of $Al_2O_3$and (c) Change in $f^{'}$ and θ for solid volume fraction of.*Cu*

$$\frac{1}{PrRe}\left(\left(1+\frac{4}{3}\frac{Rn}{B_4}\left(1+(\omega-1)\theta_{j-\frac{1}{2}}\right)^3\right)Y'\right)+\frac{1}{PrRe}\left(4\frac{Rn}{B_4}\left(1+(\omega-1)\theta_{j-\frac{1}{2}}\right)^2(\omega-1)Y_{j-\frac{1}{2}}^2\right)+\frac{B_3}{B_4}f_{j-\frac{1}{2}}Y_{j-\frac{1}{2}}+\frac{Ec}{Re}\left(\begin{array}{l}\frac{1}{B_4B}\left(4U_{j-\frac{1}{2}}^2+\delta V_{j-\frac{1}{2}}^2\right)\\ +\frac{B_2}{B_4}M^2U_{j-\frac{1}{2}}^2\end{array}\right)=0. \tag{28}$$

In third the system of algebraic equations are linearized by using Newton's method of linearization. The linearized system of equations is

$$\left.\begin{array}{l}\delta f_j-\delta f_{j-1}-\frac{h_j}{2}\left(\delta U_j+\delta U_{j-1}\right)=(r_1)_{j-\frac{1}{2}}\\ \delta U_j-\delta U_{j-1}-\frac{h_j}{2}\left(\delta V_j+\delta V_{j-1}\right)=(r_4)_{j-\frac{1}{2}}\\ \delta V_j-\delta V_{j-1}-\frac{h_j}{2}\left(\delta W_j+\delta W_{j-1}\right)=(r_5)_{j-\frac{1}{2}}\\ \delta\theta_j-\delta\theta_{j-1}-\frac{h_j}{2}\left(\delta Y_j+\delta Y_{j-1}\right)=(r_6)_{j-\frac{1}{2}}\end{array}\right\}, \tag{29}$$

$$\xi_1\delta f_j+\xi_2\delta f_{j-1}+\xi_3\delta U_j+\xi_4\delta U_{j-1}+\xi_5\delta V_j+\xi_6\delta V_{j-1}+\xi_7\delta W_j+\xi_8\delta W_{j-1}=(r_2)_{j-\frac{1}{2}}, \tag{30}$$

$$\begin{array}{l}\psi_1\delta f_j+\psi_2\delta f_{j-1}+\psi_3\delta U_j+\psi_4\delta U_{j-1}+\psi_5\delta V_j+\psi_6\delta V_{j-1}+\\ \psi_7\delta\theta_j+\psi_8\delta\theta_{j-1}+\psi_9\delta Y_j+\psi_{10}\delta Y_{j-1}=(r_3)_{j-\frac{1}{2}},\end{array} \tag{31}$$

In which

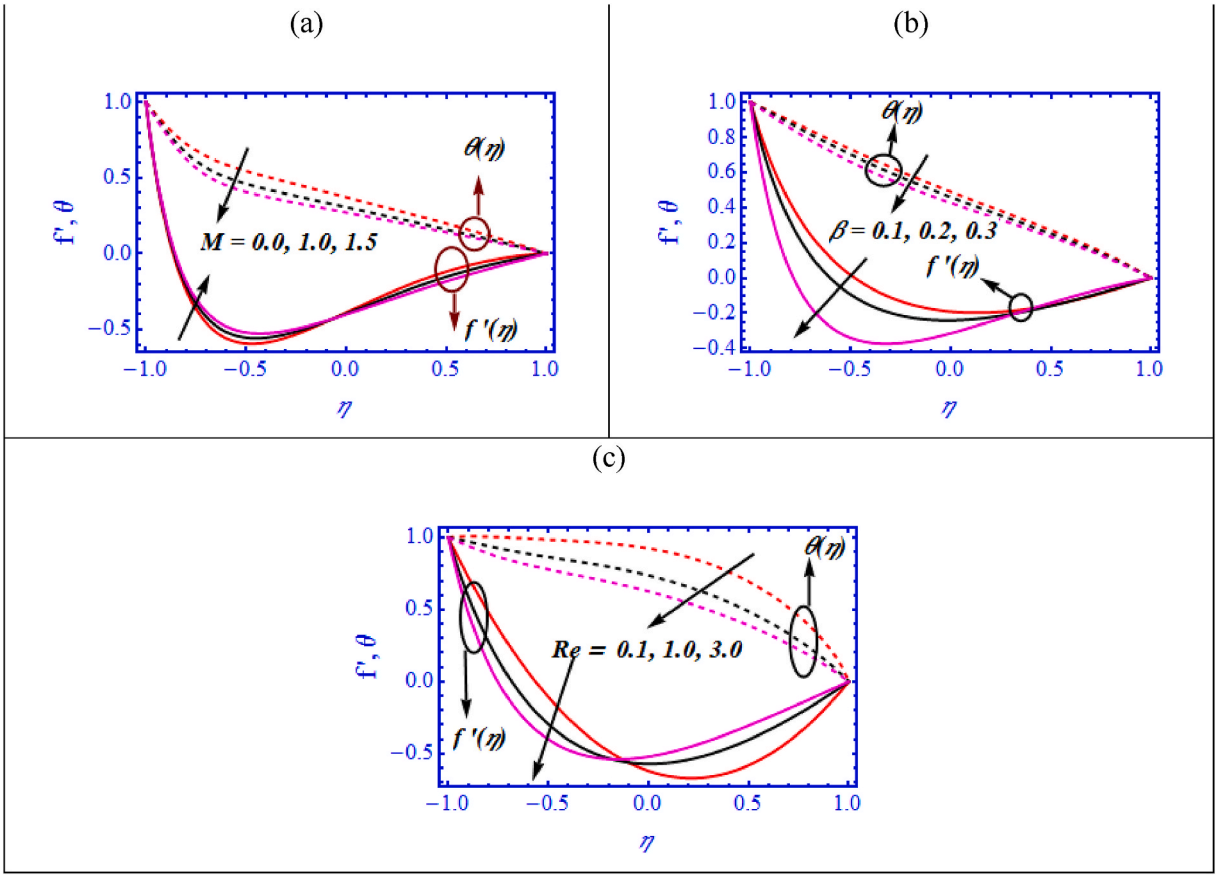

Fig. 3. (a)Change in f' and θ for M, (b)change in f' and θ forβ and (c) change in f' and θ for.Re.

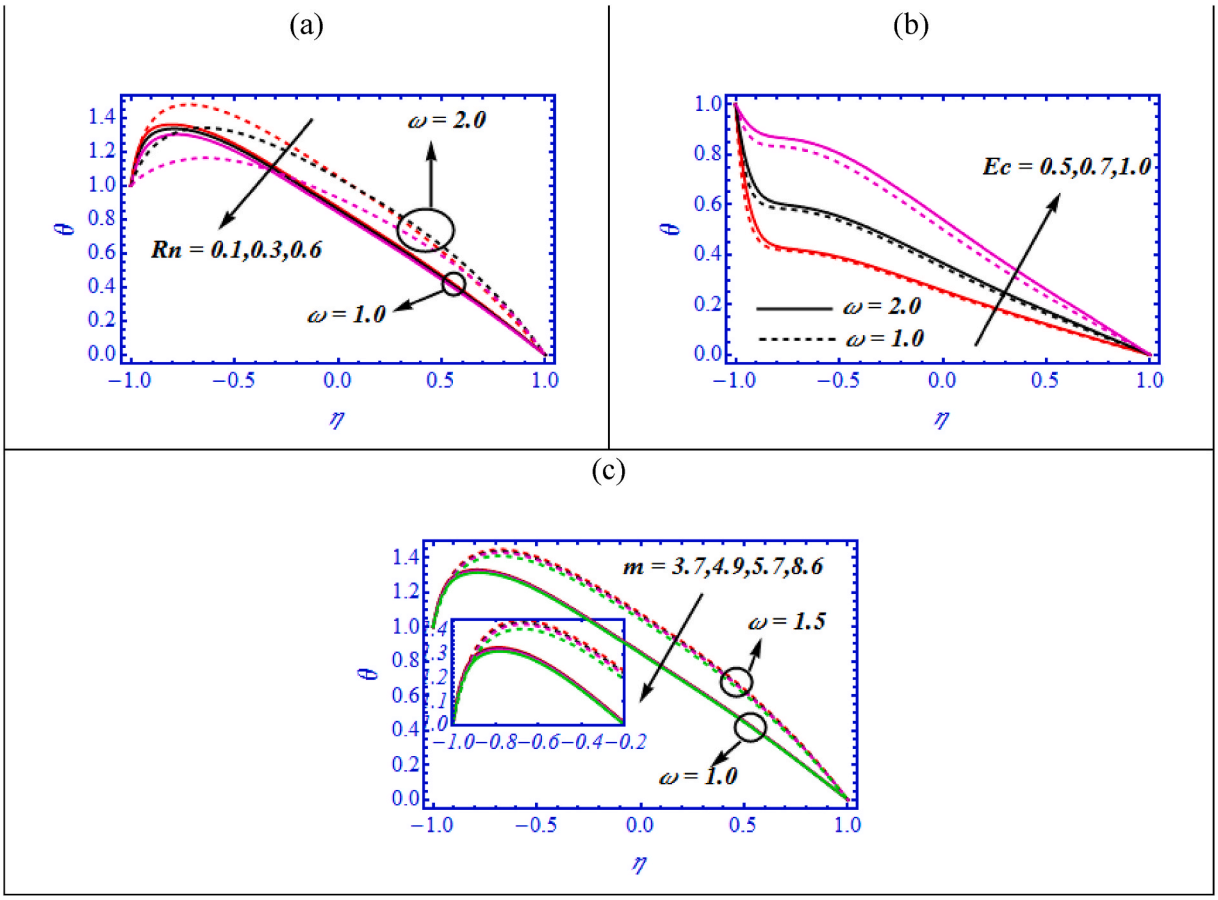

Fig. 4. (a) Change in θ due to *Rn*, (b) change in θ due to *Ec* and (c) change in θ due to.*m*

$$\left.\begin{aligned}
&\xi_1 = -\frac{h_j}{2}BB_1W_{j-\frac{1}{2}}, \quad \xi_2 = \xi_1\\
&\xi_3 = -\frac{h_j}{2}BB_1V_{j-\frac{1}{2}}, \quad \xi_4 = \xi_3\\
&\xi_5 = -\frac{h_j}{2}BB_1U_{j-\frac{1}{2}} - \frac{h_j}{2}M^2BB_2, \quad \xi_6 = \xi_5\\
&\xi_7 = 1 - \frac{h_j}{2}BB_1f_{j-\frac{1}{2}}, \xi_8 = -1 - \frac{h_j}{2}BB_1f_{j-\frac{1}{2}}\\
&\psi_1 = PrReB_3\frac{h_j}{2}Y_{j-\frac{1}{2}}, \quad \psi_2 = \psi_1\\
&\psi_3 = \frac{4PrEc}{B}h_jU_{j-\frac{1}{2}} + PrEcB_2h_jM^2U_{j-\frac{1}{2}}, \quad \psi_4 = \psi_3\\
&\psi_5 = \frac{\delta_1 PrEc}{B}h_jV_{j-\frac{1}{2}} \quad \psi_6 = \psi_5 \text{e.t.c.},
\end{aligned}\right\}, \tag{32}$$

Now in fourth step, the set of equations 29–31 are written into matrix form and block tri-diagonal technique is used to find the unknowns.

4. Validation of code

In Table 4 the present the results are presented for $f''(-1)$ with $\varphi_1 = \varphi_3 = 0.0$ i.e. (only in presence of copper nanoparticles) and compared with Raza et al. [7] for various values of φ_2. After deep analysis of table, it is observed that the present results show agreement with this analysis.

5. Results and discussion

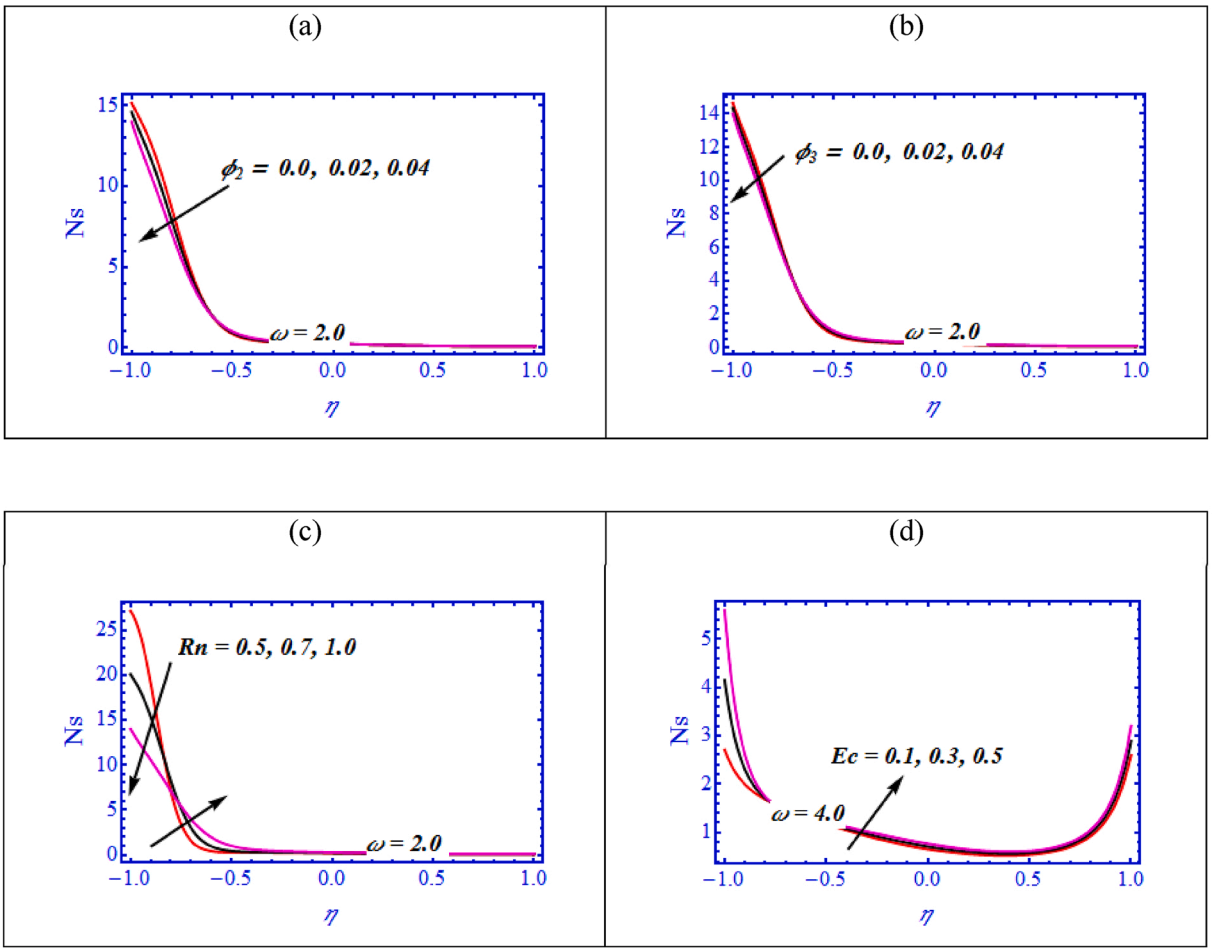

Fig. 5. (a) Change in N_s due to φ_1, (b)change in N_s due to φ_2 , (c) change in N_s due to *Rn*and (d) change in N_s due to *Ec*.
Other parameters are $Re = 10, \beta = 0.3, \Omega = 10, \mathrm{m} = 8.6, \delta_1 = 0.1$ and.$Pr = 6.2$.

In the present section the impact of various involved parameters of interest like solid volume fraction of *CuO* which is φ_1, solid volume fraction of Al_2O_3 which is φ_3, stretching Reynolds number *Re*, magnetic parameter *M*, suction parameter β, radiation

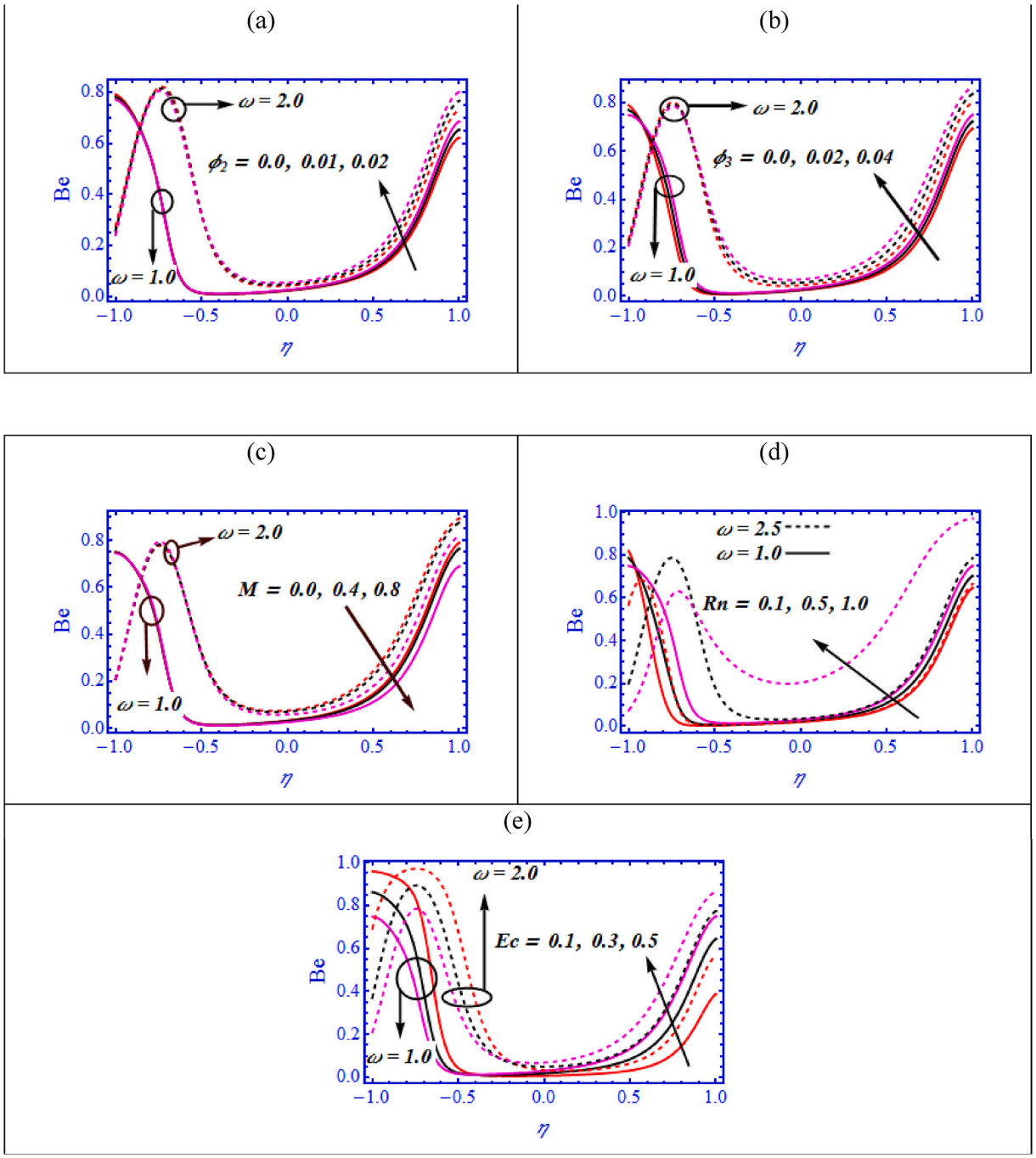

Fig. 6. (a–e): Change in *Be* due to φ_2, (b)change in *Be* due to φ_3, (c)change in *Be* due to *M*, (d)change in *Be* due to *Rn* and (e) change in *Be* due to *Ec*. Other parameters are $Re = 10, \beta = 0.3, \Omega = 1.0, \mathrm{m} = 8.6, \delta_1 = 0.1$ and.$Pr = 6.2$.

$$
\left.
\begin{aligned}
(r_1)_{j-\frac{1}{2}} &= f_{j-1} - f_j + h_j U_{j-\frac{1}{2}} \\
(r_2)_{j-\frac{1}{2}} &= W_{j-1} - W_j + B_1 BRe h_j U_{j-\frac{1}{2}} V_{j-\frac{1}{2}} \\
&\quad + B_1 BRe h_j f_{j-\frac{1}{2}} W_{j-\frac{1}{2}} + M^2 BB_2 h_j V_{j-\frac{1}{2}} \\
(r_3)_{j-\frac{1}{2}} &= \left(B_4 + (\omega-1)^3 \theta^3_{j-\frac{1}{2}} + 3(\omega-1)\theta_{j-\frac{1}{2}} + 3(\omega-1)^2 \theta^2_{j-\frac{1}{2}}\right)\frac{4}{3} Rn\left(Y_{j-1} - Y_j\right) \\
&\quad - \left(4Rnh_j\left((\omega-1) + (\omega-1)^3 \theta^2_{j-\frac{1}{2}} + 2(\omega-1)^2 \theta_{j-\frac{1}{2}}\right) Y^2_{j-\frac{1}{2}}\right) - PrReB_3 h_j f_{j-\frac{1}{2}} Y_{j-\frac{1}{2}} \\
&\quad - h_j \frac{4PrEc}{B}\left(U_{j-\frac{1}{2}}\right)^2 - h_j \frac{\delta_1 PrEc}{B}\left(V_{j-\frac{1}{2}}\right)^2 - PrEcB_2 h_j M^2 \left(U_{j-\frac{1}{2}}\right)^2 \\
(r_4)_{j-\frac{1}{2}} &= U_{j-1} - U_j + h_j V_{j-\frac{1}{2}} \\
(r_5)_{j-\frac{1}{2}} &= V_{j-1} - V + h_j W_{j-\frac{1}{2}} \\
(r_6)_{j-\frac{1}{2}} &= \theta_{j-1} - \theta_j + h_j \theta_{j-\frac{1}{2}}
\end{aligned}
\right\}, \quad (33)
$$

(33)

parameter *Rn*and viscous dissipation *Ec*on similarity axial velocity profile $f'(\eta)$, temperature profile $\theta(\eta)$ is displayed, entropy generation number and Bejan number is plotted. The temperature profile, entropy generation number and Bejan number are also presented for linear and non-linear radiations for various shapes of nanoparticles. The tabular data for skin fraction and Nusselt number is calculated and presented for Cu, CuO nanofluid, Al_2O_3 nanofluid and $(Cu + CuO + Al_2O_3)$modified hybrid nanofluid for various values of penetrating parameters. The values of parameters are taken fixed as $M = 0.5$, $Re = 10, \beta = 0.5, Ec = 2.0, \delta_1 = 0.5, Pr = 6.2$, $Rn = 1.0, \omega = 2.0$, $\varphi_1 = \varphi_2 = 0.04, 0$ and. $\varphi_3 = 0.04$. Tables 5 and 6 respectively highlights the impact of various flow parameters on the engineering quantities e.g skin friction coefficient and Nusselt numbers.

The similar velocity $f'(\eta)$ and temperature $\theta(\eta)$ is plotted in Fig. 2(a) by varying the solid volume fraction of *CuO* nanoparticles. It is noted that increase in solid volume fraction of copper oxide nanoparticles improve the velocity of $(Cu + CuO + Al_2O_3)$ modified hybrid nanofluid in upper half region of the channel while opposite trend is followed in lower half of the channel. The temperature is a rises by increases function of solid volume fraction of *CuO* nanoparticles. Furthermore, copper oxide has small rise in temperature as compared to the rise in temperature against *Cu*. Which indicates that temperature for *Cu* nanoparticles declines which is clear in Fig. 2(c). From Fig. 2(b) it is clear that the trend of velocity profile against the solid volume fraction of Al_2O_3 nanoparticles is similar in trend against *Cu* and *CuO* nanoparticles in both halves of the channel. When the concentration of Al_2O_3 nanoparticles increases the fractional forces which decrease the viscosity of the fluid as a consequence the motion of the fluid is resisted in lower region of the channel. The temperature of modified nanofluid also rises but this rise is small in magnitude as compared to the rise due to solid fraction of *Cu* and *CuO*. Due to rises in temperature due to solid volume fraction of Cu, CuO and Al_2O_3 nanoparticles, this modified model has many applications in thermal management devices and nuclear reactor. The impact of magnetic parameter on the velocity and temperature is plotted and discussed through Fig. 3(a). The decline in velocity of modified nanofluid in the upper half region of the channel while as we move towards lower half the reverse behavior can be observed with increasing magnetic parameter. As we know that the Lorentz force is resistive force which oppose the transport of modified nanofluid in axial direction so as a result velocity of the fluid decreases in the upper half of the channel. The increase of velocity in lower half of the channel is observed due to the stretching of the lower wall with constant speed. The temperature of nanofluid rises when we increase the strength of magnetic field. When we increase the strength of magnetic force, the generation of eddy current occur in the transportation of nanofluid which rises temperature of nanofluid and clearly depicted in Fig. 3(a). Both axial velocity and temperature of the fluid under the action of suction parameter β is observed in Fig. 3(b). The velocity of modified nanofluid declines in the lower half of the channel while rises near the upper wall of the channel for large values. It is observed that temperature profile increases throughout the channel as we increase the suction parameter. As the lower wall is permeable so velocity decreases in the lower half and increases in the upper half with rising amplitude. Fig. 3(c) is demonstration of the response of velocity profile $f'(\eta)$ and temperature profile $\theta(\eta)$ against the growing values of stretching Reynolds number. It is noticed that the velocity decreases near the stretched wall and permeable wall while increases with growing magnitude in the rest region of the channel. The fall in temperature in the whole channel is noticed for the rising values of Reynolds number. The effects of radiation parameter *Rn* on temperature distribution $\theta(\eta)$ is plotted in Fig. 4(a) for both linear and non-linear Radiative flows. The fall in temperature is noticed with increasing values of *Rn*. Furthermore, the decreasing magnitude is large for non-linear Radiative flow as compared to linear Radiative flow. The fall in temperature distribution occur due to the effective loss in the kinetic energy of the nanoparticles in the suspension in Radiative flow. Furthermore, non-linear Radiative flow occur due to temperature ratio parameter. Increase in temperature ratio parameter also corresponds to the loss in energy which results in the fall in temperature distribution of the fluid. From Fig. 4(b) the rise in the temperature with increase in Eckert number can be seen and roundabout in temperature curves is dominant for large values of *Ec* for various values of ω.Since Eckert number and internal kinetic energy of considered fluid has direct relation and rise in Eckert number cause a boost in kinetic energy. As a result the amplitude of temperature is higher for larger values of *Ec*. The impact of shape factor on the temperature of modified nanofluid for dissimilar values of ω is plotted in Fig. 4(c). It is noted that the shape factor decrease the temperature of modified nanofluid for both linear and non-linear radiations. Furthermore, for non-linear radiation the decrease in temperature is dominant.

Fig. 5(a–d) are plotted to report and analyze the outcomes of volume fraction of Cu, solid volume fraction of Al_2O_3 which is φ_3, radiation parameter *Rn* and Ecker number *Ec* on entropy generation number in non-linear Radiative flow. The entropy generation reduces by improving the solid volume fraction of *Cu* and Al_2O_3 nanoparticles near the stretched and permeable wall. These effects vanish as move the profile is analyzed away from lower wall. It is understood effect that the effects of volume fraction of nanoparticles on entropy generation number are dominant near the wall due to stretching and suction effects.

The rise in radiation parameter diminish the entropy generation number near the lower wall of the channel. The development in thermal and momentum boundary layer occur due to the release in heat energy to the fluid by thermal radiation. Hence, for larger values of radiation parameter the entropy profile rises away from the wall. The optimization in the entropy generation is probably due to the permeable and stretching wall. .The rise in Eckert number strengthens the entropy generation number for hybrid nanofluid in the entire channel. Furthermore, these effects are dominant near the stretched wall and optimized in the rest region of the channel.

The significances of solid volume fractions of *Cu* and Al_2O_3 which is φ_2 and φ_3 respectively, magnetic parameter(M), radiation parameter(Rn) and viscous parameter(Ec) on the Bejan number for various values of temperature ratio parameter ωin Fig. 6(a–e). The solid volume fraction of *Cu* as well as Al_2O_3 diminish the Bejan number in the in lower half of the channel. Furthermore, the decreases is more dominant in case of non-linear radiation parameter. The Bejan number increases near the upper wall of the channel with large magnitude for $\omega = 2.0$. The Bejan number is a decreasing function of magnetic parameter M for both values of temperature ratio parameter ω. The radiation phenomena increases the Bejan number for several values of ω. It is also clear that increasing trend against the increasing values of *Rn* is large in magnitude in case of $\omega = 2.5$ which describing the non-linear radiation phenomena. The rise in viscous dissipation also growths the Bejan number near the stretching wall while Bejan number shrinks in the rest region of the

channel. In order to optimize and control the heat transfer effects in different features of heat transfer viscous dissipation play important character in the stretching and blowing environment.(see Table 6)

6. Concluding remarks

The flow of hybrid nanofluid with heat transfer characteristics is computed numerically in the present study. The effects of suction parameter, stretching Reynolds number, Magnetic parameter, Eckert number, radiation parameter and heat source/sink parameter are analyzed graphically on velocity of fluid, temperature of the fluid, entropy generation number and Bejan number. The impact of emerging parameters on the skin fraction and Nusselt number is reported and compared for $Cu + Al_2O_3$ hybrid nanofluid and modified nanofluid. Also Nusselt number is tabulated for linear and non-linear Radiative flow.

1 The solid volume fraction of the nanoparticles cause a notable variation of velocity in lower and upper half of the channel.
2 The temperature of the nanofluid has decreasing function of radiation parameter.
3 Temperature profile decreases with suction parameter, magnetic force and stretching Reynolds number.
4 The solid volume fraction of Cu and Al_2O_3 declines entropy generation number near the lower wall of the permeable channel.
5 The Bejan number increases by enhancing solid volume fraction of nanoparticles and radiation parameter in upper half of the channel.

Declaration of competing interest

The authors declare that they have no known competing financial interests or personal relationships that could have appeared to influence the work reported in this paper.

Acknowledgment

The authors extend their appreciation to the deanship of scientific research at King Khalid University for funding this work through research group program under grant number (R.G.P. 1/327/42).

References

[1] Mustafa Turkyilmazoglu, Exact multiple solutions for the slip flow and heat transfer in a converging channel, Oct, J. Heat Tran. 137 (10) (2015), 101301, 8.
[2] Saleem Asghar, Mudassar Jalil, Muhammad Hussan, Mustafa Turkyilmazoglu, Lie group analysis of flow and heat transfer over a stretching rotating disk, Int. J. Heat Mass Tran. 69 (2014) 140–146. February.
[3] Mustafa Turkyilmazoglu, Latitudinally deforming rotating sphere, Appl. Math. Model. 71 (July 2019) 1–11.
[4] S.U.S. Choi, Enhancing thermal conductivity of fluids with nanoparticles, ASME-Publ. Fed. 231 (1995) 99–106.
[5] G.K. Ramesh, G.S. Roopa, Sabir Ali Shehzad, S.U. Khan, Interaction of Al2O3-Ag and Al2O3-Cu hybrid nanoparticles with water on convectively heated moving material, Multidiscip. Model. Mater. Struct. 16 (6) (2020) 1651–1667.
[6] S. Ahmad, S. Nadeem, Analysis of activation energy and its impact on hybrid nanofluid in the presence of Hall and ion slip currents, Appl. Nanosci. 10 (12) (2020) 5315–5330.
[7] J. Raza, A.M. Rohni, Z. Omar, MHD flow and heat transfer of Cu–water nanofluid in a semi porous channel with stretching walls, Int. J. Heat Mass Tran. 103 (2016) 336–340.
[8] K. Gangadhar, T. Kannan, P. Jayalakshmi, Magnetohydrodynamic micropolar nanofluid past a permeable stretching/shrinking sheet with Newtonian heating, J. Braz. Soc. Mech. Sci. Eng. 39 (2017) 4379–4391.
[9] K. Gangadhar, K. Kukkamalla, S.M. Ibrahim, Effect of thermal radiation on engine oil nanofluid flow over a permeable wedge under convective heating: Keller box method, Multidiscip. Model. Mater. Struct. 15 (1) (2019) 187–205.
[10] B. Ali, S. Hussain, Y. Nie, A.U. Rehman, M. Khalid, Buoyancy effects on falknerskan flow of a Maxwell nanofluid fluid with activation energy past a wedge: finite element approach, Chin. J. Phys. 68 (2020) 368–380.
[11] Kh Hosseinzadeh, So Roghani, A.R. Mogharrebi, A. Asadi, M. Waqas, D.D. Ganji, Investigation of cross-fluid flow containing motile gyrotactic microorganisms and nanoparticles over a three-dimensional cylinder, Alexandria Eng. J. 59 (Issue 5) (October 2020) 3297–3307.
[12] Ying-QingSong, ShanAli Khan, Muhammad Imran, Waqas Hassan, Sami Ullah Khan, M. Ijaz Khan, Sumaira Qayyum, Yu-Ming Chu, Applications of modified Darcy law and nonlinear thermal radiation in bioconvection flow of micropolar nanofluid over an off centered rotating disk, Alexandria Eng. J. 60 (Issue 5) (October 2021) 4607–4618.
[13] Kotha Gangadhar, Venkata Ramana Kolipaula, Munagala Venkata Subba Rao, Surekha Penki, J. Ali, Chamkha , Internal heat generation on bioconvection of an MHD nanofluid flow due to gyrotactic microorganisms, Eur. Phys. J. Plus 135 (2020), 600.
[14] K. Dasaradha Ramaiah, P. Surekha, Gangadhar Kotha, Thangavelu Kannan, MHD rotating flow of a Maxwell fluid with Arrhenius activation energy and non-Fourier heat flux model, Heat Tran. Asian Res. 49 (4) (2020) 2209–2227. June.
[15] K. Gangadhar, T. Kannan, G. Sakthivel, K. DasaradhaRamaiah, Unsteady free convective boundary layer flow of a nanofluid past a stretching surface using a spectral relaxation method, Int. J. Ambient Energy 41 (6) (2020) 609–616.
[16] Mustafa Turkyilmazoglu, Nanoliquid film flow due to a moving substrate and heat transfer, Eur. Phys. J. Plus 135 (2020), 781.
[17] A. Bejan, A study of entropy generation in fundamental convective heat transfer, J. Heat Tran. 101 (1979) 718–725.
[18] M. Ijaz, M. Ayub, H. Khan, Entropy generation and activation energy mechanism in nonlinear radiative flow of Sisko nanofluid: rotating disk, Heliyon 5 (2019), e0186.
[19] Kh Hosseinzadeha, A. Asadi, A.R. Mogharrebi, Javad Khalesi, Seyedmohammad Mousavisani, D.D. Ganji, Entropy generation analysis of (CH2OH)2 containing CNTs nanofluid flow under effect of MHD and thermal radiation, Case Stud. Therm. Eng. 14 (2019), 10048.
[20] M.K. Nayak, S. Shaw, M. Ijaz Khan, O.D. Makinde, Yu-MingChu, Sami Ullah Khan, Interfacial layer and shape effects of modified Hamilton's Crosser model in entropy optimized Darcy-Forchheimer flow, Alexandria Eng. J. 60 (Issue 4) (2021) 4067–4083. August.
[21] Mair Khan, Amna Shahid, M. El Shafey, T. Salahuddin, Farzana Khan, Predicting entropy generation in flow of non-Newtonian flow due to a stretching sheet with chemically reactive species, Comput. Methods Progr. Biomed. 187 (2020) 105246.
[22] M Zubair Akbar Qureshi, S. Bilal, M. Bila Ameen, Tahir Mushtaq, M.Y. Malik, Numerical examination about entropy generation in magnetically effected hybridized nanofluid flow between orthogonal coaxial porous disks with radiation aspects, Surf. Interfaces 26 (2021), 101340. October.

[23] Yong-Min Li, M. Ijaz Khan, Sohail A. Khan, Sami Ullah Khan, Zahir Shah, Poom Kumam, an assessment of the mathematical model for estimating of entropy optimized viscous fluid flow towards a rotating cone surface, Sci. Rep. 11 (2021), 10259.
[24] Priyajit Mondal, T.R. Mahapatra, MHD double-diffusive mixed convection and entropy generation of nanofluid in a trapezoidal cavity, Int. J. Mech. Sci. 208 (2021), 106665, 15 October.
[25] Abuzar Ghaffari Usman, Irfan Mustafa, Taseer Muhammad, Yasir Altaf, Analysis of entropy generation in a power-law nanofluid flow over a stretchable rotatory porous disk, Case Stud. Therm. Eng. 28 (2021), 101370. December.
[26] Samina Batool, , Bushra Khatoon Siddiqui, M.Y. Malik, A.S. Alqahtani, Qazi Mahmood ul Hassan, Double diffusion in stretched flow over a stretching cylinder with activation energy and entropy generation, Case Stud. Therm. Eng. 26 (2021), 101119. August.
[27] A. Sattar Dogonchi, M.S. Sadeghi, M. Ghodrat, Ali J. Chamkha, Yasser Elmasry, Alsulami Radi, Natural convection and entropy generation of a nanoliquid in a crown wavy cavity: effect of thermo-physical parameters and cavity shape, Case Stud. Therm. Eng. 27 (2021), 101208. October.
[28] Hu Ge-JiLe, Sumaira Qayyum, Faisal Shah, M Ijaz Khan, Sami Ullah Khan, Slip flow of Jeffrey nanofluid with activation energy and entropy generation applications, Adv. Mech. Eng. 13 (3) (2021) 1–9, 2021.
[29] M.I. Khan, F. Alzahrani, A. Hobiny, Z. Ali, Modeling of Cattaneo-Christov double diffusions (CCDD) in Williamson nanomaterial slip flow subject to porous medium, J. Mater. Res. Technol. 9 (2020) 6172–6177.
[30] M.I. Khan, F. Alzahrani, A. Hobiny, Z. Ali, Fully developed second order velocity slip Darcy-Forchheimer flow by a variable thicked surface of disk with entropy generation, Int. Commun. Heat Mass Tran. 117 (2020), 104778.
[31] M.I. Khan, F. Alzahrani, Nonlinear dissipative slip flow of Jeffrey nanomaterial towards a curved surface with entropy generation and activation energy, Math. Comput. Simulat. 185 (2021) 47–61.
[32] M.I. Khan, S. Qayyum, T. Hayat, M.I. Khan, A. Alsaedi, Entropy optimization in flow of Williamson nanofluid in the presence of chemical reaction and Joule heating, Int. J. Heat Mass Tran. 133 (2019) 959–967.
[33] T. Hayat, N. Aslam, M.I. Khan, M.I. Khan, A. Alsaedi, Physical significance of heat generation/absorption and Soret effects on peristalsis flow of pseudoplastic fluid in an inclined channel, J. Mol. Liq. 275 (2019) 599–615.